Soft Matter

PAPER

View Article Online
View Journal | View Issue

Shooting in a foam

Anne Le Goff,†*[a] David Quéré[a] and Christophe Clanet[b]

Cite this: *Soft Matter*, 2014, **10**, 6696

Received 27th February 2014
Accepted 23rd June 2014

DOI: 10.1039/c4sm00457d

www.rsc.org/softmatter

We study the motion of a solid sphere after its fast impact on a bath of liquid foam. We identify two regimes of deceleration. At short times, the velocity is still large and the foam behaves similar to a Newtonian fluid of constant viscosity. Then we measure a velocity threshold below which the sphere starts experiencing the foam's elasticity. We interpret this behavior using a visco-elasto-plastic model for foam rheology. Finally we discuss the possibility of stopping a projectile in the foam, and evaluate the capture efficiency.

1 Introduction

A liquid foam consists of a closely packed suspension of gas bubbles in a continuous liquid phase. Because of their remarkable mechanical properties (solid-like at rest and liquid-like under shear), foams have attracted the attention of physicists from the early work of Plateau[1] to modern debates on the jamming of soft materials.[2,3] Foams are also widely used in diverse industrial fields: catalysis and filtration,[4] flotation,[5] and shock or noise absorption.[6] The cellular structure of foams governs many of their properties, such as shear modulus or yield stress, that scale with the Laplace pressure inside the bubbles[7] with an influence of the topology of the bubble assembly.[8]

Solid cellular materials are known as mechanical dampers and sound absorbers. In nature, it has been shown recently that woodpeckers have porous cranial bones that prevent their brain from injury in spite of repeated head drumming against tree trunks,[9] and that the thick skin that protects pomelos when they fall off the tree has a foam-like structure.[10] The use of solid foams as mechanical dampers in technology is widespread, even under extreme conditions: for example, to capture interstellar particles without damage, which travel at high velocity, soft solids called aerogels are used.[11] In this spirit, we investigate the ability of liquid foams to absorb kinetic energy.

To do so, we measure the energy dissipation during the impact of a solid sphere of radius R_0 and initial velocity V_0. We restrict our study to projectiles much larger than the foam bubbles, and to characteristic impact times $\tau_c = R_0/V_0$ much shorter than the foam rearrangement time τ_r. This regime corresponds to region I in the phase diagram represented in Fig. 1, where the vertical axis compares the projectile size R_0 to the foam bubble radius r_b and the horizontal axis compares the rearrangement and impact times, τ_r and τ_c. Other regions of this phase diagram have been explored in the literature: regions II and III correspond to the case of foams whose bubbles are much larger than solid particles. When they are fast, small projectiles can cross the soap films separating neighboring bubbles.[12] Else, they stay trapped in the nodes where Plateau borders meet.[13] In region IV, quasi-static foam flows around an obstacle, whose dimension is one order of magnitude higher than bubble size, are studied in 2D[14] and 3D.[15] The experimental setup dedicated to the study of region I is described in Section 2, results are presented in Section 3, and a model is developed in Section 4.

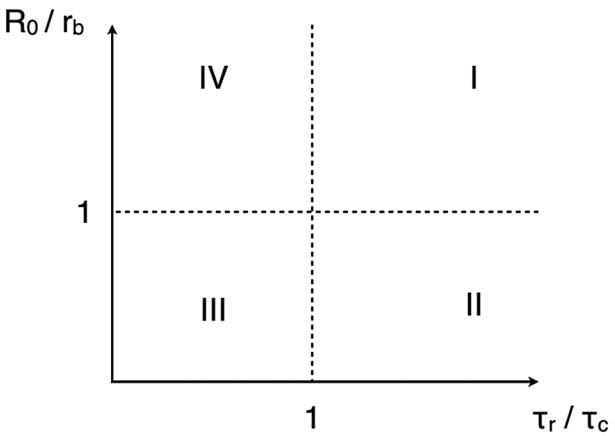

Fig. 1 Phase diagram for foam-projectile interactions. On the vertical axis, the typical size of the solid object R_0 is compared to the radius r_b of bubbles in the foam. On the horizontal axis, the time scale τ_r of bubble rearrangements is compared to the characteristic time scale for impact $\tau_c = R_0/V_0$. This study focuses on the impact of fast projectiles larger than foam bubbles: our region of interest is the upper right corner of this phase diagram (region I).

2 Experimental setup

The experimental setup is presented in Fig. 2: spheres of different radius R_0 and density ρ_s are thrown at velocity V_0 in a foam trapped in a tube of radius R_T.

[a]*PMMH, UMRS 7636 du CNRS, ESPCI, 75005 Paris, France*

[b]*LadHyX, UMR 7646 du CNRS, École Polytechnique, 91128 Palaiseau, France*

† Present address: BMBI, UMR 7338 du CNRS, Université de Technologie de Compiègne, 60200 Compiègne, France. E-mail: anne.le-goff@utc.fr.

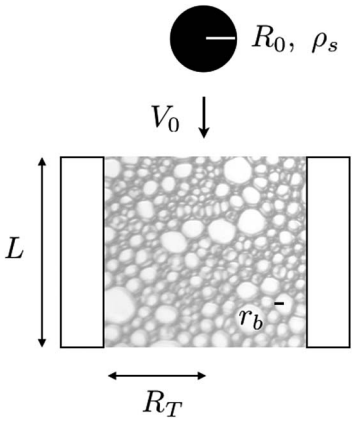

Fig. 2 Sketch of the experiment (drawing not to scale).

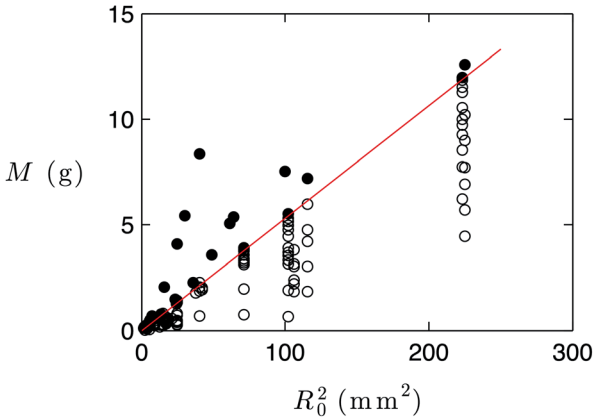

Fig. 3 Phase diagram showing the behavior of spheres of mass M and radius R_0 gently deposited at the surface of the foam. After 5 minutes, some spheres sink under their own weight (●), others stay at the surface (○). The solid line represents the transition between the two regimes.

2.1 Foam

For the foam, we use a well-characterized Gillette shaving cream:[16] the foaming solution has a surface tension $\gamma = 29.6$ mN m^{-1} and a viscosity $\eta = 1.9$ mPa s, yet shown to vary from one sample to another, sometimes being as high as 5 mPa s.[17] Due to aging, bubble size and related properties evolve with time:[18] to avoid such effects, experiments are performed 20 minutes after blowing the foam. At this moment, we directly observe under a microscope that the bubble radius is $r_b = 21 \pm 3$ μm. The liquid volume fraction Φ_l is about 7.5% and does not vary over the time of our experiment.

2.2 Choice of spheres

Our purpose is to stop projectiles using a foam, so we first need to check that they can indeed get stuck in foam. To do so, we gently deposit spheres at the top surface of a tank filled with foam and observe their behavior for 5 minutes. Spheres that sink over a distance equal or superior to their diameter are counted as "sinking", others are labelled as "floating". Fig. 3 presents the phase diagram obtained when the mass M and the radius R_0 of the sphere are varied independently. Floating spheres are represented by hollow symbols, sinking spheres by black ones. For this experiment, we use both plain spheres and hollow ones progressively filled with lead particles until they sink. We observe in Fig. 3 that for each radius there is a critical mass M_c above which the sphere sinks. This critical mass increases linearly with the surface area, following the heuristic behavior $M_c/{R_0}^2 = 56 \pm 1$ kg m^{-2}.

The behavior of the sphere results from a balance between its weight and the foam's elastic response. Projected on a vertical axis, this balance can be written $M_g = \pi {R_0}^2 \sigma$, where σ is the average stress. At the limit of yielding, the value of the stress reaches the foam yield stress $\sigma = \sigma_Y$. For a given sphere radius, this characterizes a critical mass $M_c = \pi {R_0}^2 \sigma_Y / g$. From the data in Fig. 3, we extract $\sigma_Y \simeq 170$ Pa. This is about four times larger than the values published in the literature and obtained by oscillatory rheometry.[19] This can be explained by the relatively short waiting time of 5 minutes after which our spheres are sorted in two categories. A sphere counted as "floating" after 5 minutes may sink between 5 and 10 minutes. It was pointed out by Barnes that yield stress is an ambiguous quantity whose value is likely to depend on the shear rate range, and even to vanish when measured at extremely low shear rates.[20] The discrepancy between our crude measurement and the results obtained from non-linear rheology may be explained by the fact that we are doing a static interpretation of a phenomenon that occurs over a finite time span.

In the finite velocity impact experiments described below, we only use spheres defined as "floating" in Fig. 3 ($M < M_c$), for which the foam yield stress exceeds, sometimes by far, the pressure induced by their own weight. The spheres are made of different materials: stainless steel ($\rho_s = 8000$ kg m^{-3}), glass ($\rho_s = 2580$ kg m^{-3}), polypropylene ($\rho_s = 920$ kg m^{-3}) and polyacetal ($\rho_s = 1400$ kg m^{-3}). In order to reach intermediate values of density, we also prepared non-homogeneous spheres by embedding lead particles into a soft polymer matrix. The radius of the spheres, R_0, ranges from 2 mm to 6.4 mm. The sphere's properties are summarized in Table 1. The whole study is conducted in the limit $r_b \ll R_0 \ll R_T$.

2.3 Launching systems and tubes

Concerning the impact velocity, two different types of launching have been used: the classical free fall for $V_0 \leq 5$ m s^{-1}, and a slingshot for larger velocities: $10 \leq V_0 \leq 50$ m s^{-1}. The slingshot consists of a forked stick, whose arms are connected to a pocket by two rubber bands. The average tension in the rubber bands determines the impact velocity. A difference in tension between the two bands induces a torque, making the projectile spin. In the experiments considered here, both rubber bands are stretched in a symmetric way in order to avoid spin. As a foam container, we use plexiglass tubes of internal radius $R_T = 35$ mm and length L varying between 3 and 15 cm.

All experiments are recorded using a high speed camera (Phantom V9) at a frequency of 2000 to 5000 frames per second. Image analysis is performed using ImageJ software.

Table 1 Properties of the spheres used in the experiments. Spheres are made either of raw materials (plastic or glass) or of lead particles dispersed in a soft polymer matrix (composite 1 to 4). Only three of the smallest spheres were used for high-speed experiments. In the last column, we compute the characteristic impact time $\tau_c = R_0/V_0$. τ_c always stays smaller than the typical relaxation time after a plastic event in a Gillette foam ($\tau_r \simeq 200$ ms)

Material	ρ_s (kg m^{-3})	R_0 (mm)	Free fall	Slingshot	τ_c (ms)
Polypropylene	920	2.4	×	×	0–1
Polypropylene	920	3.55	×	×	0–2
Polypropylene	920	5	×		2–4
Polyacetal	1400	3.55	×		1–2
Glass	2580	2		×	0–1
Glass	2580	3.1	×		1–3
Composite 1	2380	2.2	×		0–1
Composite 2	2990	2.8	×		0–1
Composite 3	2220	3.8	×		1–3
Composite 4	1860	6.4	×		3–7

3 Experimental results

3.1 Low velocity impact

Fig. 4 shows the impact of a sphere released above the tank and freely falling on the foam surface. The whole process is recorded by the high speed camera: as can be observed in (a), the sphere entirely penetrates the foam and is captured below the surface. To measure its position, we equipped the sphere with a flag attached to a rigid elongated tail, made out of a pulled glass capillary. Because this rod is very thin and hollow, its mass is negligible compared to that of the sphere. During the impact, the flag remains above the foam and we extract the trajectory from the evolution of its position z_f. Such a trajectory is presented in Fig. 4(b), which reveals both an oscillation and a strong damping. These features are discussed in Section 4.

3.2 High velocity impact

At high impact velocity, the sphere can cross the whole sample and escape from the foam cylinder. We throw spheres with an initial velocity V_0 on foam samples of various thicknesses L. After crossing a tube of length L_1 full of opaque foam in the time interval t_1, a sphere has decelerated from V_0 to V_1. This provides us with a new way to get a deceleration curve $V(t)$ by gathering several high speed experiments. The method is presented in Fig. 5(a), and an example of a deceleration curve is shown in Fig. 5(b) and (c). We assume that if the same sphere is crossing a longer tube $L_2 > L_1$, a process that will require a longer time $t_2 > t_1$, its velocity at the time t_1 is again V_1. We iterate this experiment using tubes of increasing length, until one of them is long enough to make the final velocity below 5 m s^{-1}. This allows us to connect data acquired through open tube experiments to those obtained from a free fall experiment by matching impact and exit velocities of different experiments. This connection is visible on the typical curve presented in Fig. 5(b): data points are more regularly spaced at low velocity than those at the beginning of the curve. This is due to the measurements at high velocity being a reconstructed curve, while data at low velocity come from a single experiment, where the time interval is fixed by camera settings.

3.2.1 Results on the initial deceleration. Qualitative statements about deceleration in foam can be drawn from a curve such as the one presented in Fig. 5(b). It takes 20 ms and less than 20 cm for a polypropylene sphere ($R_0 = 2.4$ mm) arriving at 34 m s^{-1} to slow down to 1 m s^{-1}. In a viscous oil ($\eta_{oil} = 1$ Pa s $= 1000\eta_{water}$), the same process takes about 5 ms and 3 cm.[21] In comparison, given its small liquid fraction, foam proves to be an efficient kinetic energy absorber. The energy dissipated during these initial 20 ms is about 35 mJ, corresponding to a power of almost 2 W, similar to that of a night light.

As can be seen in Fig. 5(c), the same data plotted on a semi-logarithmic graph reveal that velocity decreases exponentially with time during the first 15 ms of motion, over more than one order of magnitude. This is consistent with a Newtonian description of the foam, with an apparent viscosity η_e that can be deduced from the time scale of the exponential decay. The equation of motion for an object decelerating due to viscous friction is $M\frac{dV}{dt} = -6\pi R_0 \eta_e V$ and its integration leads to

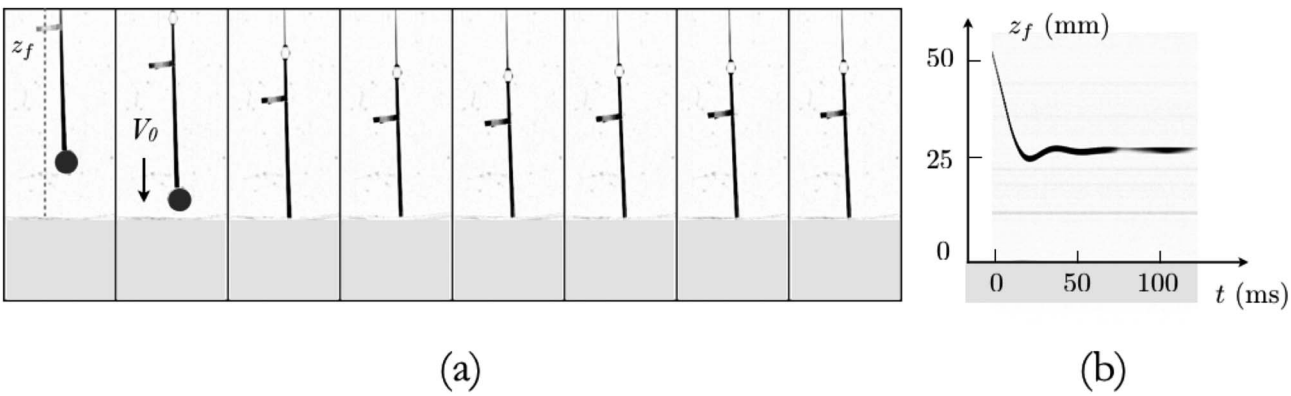

Fig. 4 (a) Chronophotography of a low velocity impact. The projectile, consisting of a glass sphere ($R_0 = 3.1$ mm) with a rod and a flag attached to it, is released about 30 centimeters above the foam surface, hitting it at 1.7 m s^{-1}. The time interval between two images is $\Delta t = 6$ ms. The position z_f of the flag is recorded during the free fall. (b) Spatiotemporal diagram showing the position z_f of the flag as a function of time.

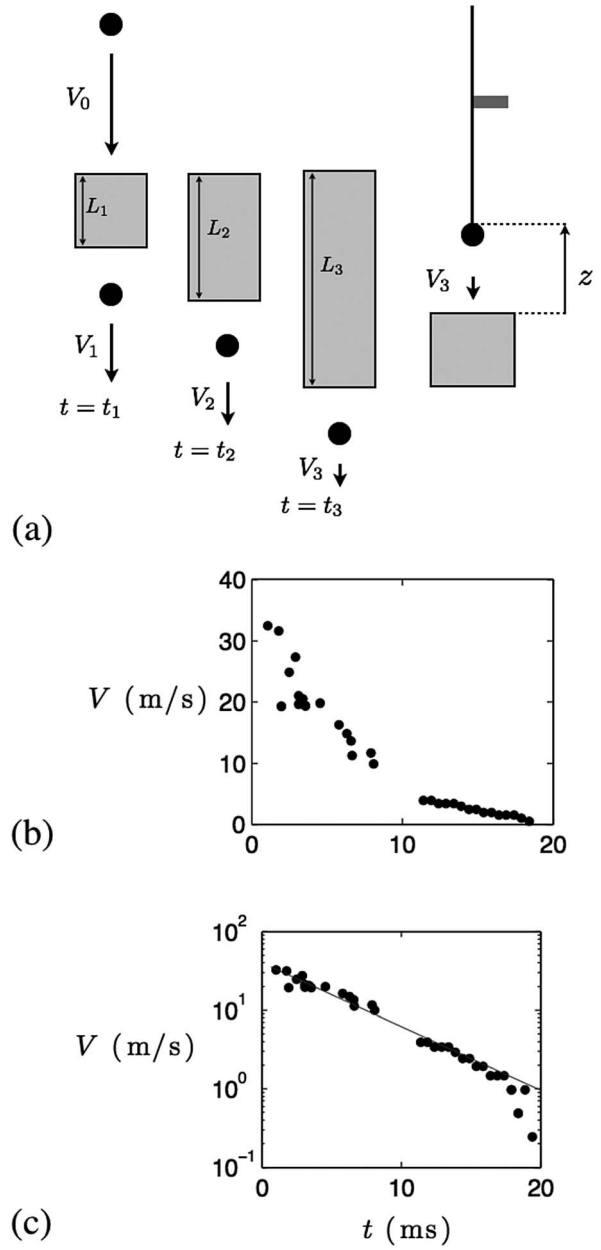

Fig. 5 (a) Principle of construction of the deceleration curves. At high velocity, each data point represents an independent experiment, one of which having a final velocity of 4 m s^{-1}. These points are then connected with measurements made on a single low velocity experiment, in which a sphere with a flag was released above the foam, reaching 4 m s^{-1} at the time of impact. (b) Example of a reconstructed deceleration curve obtained with polypropylene spheres (R_0 = 2.4 mm). (c) Semi-logarithmic representation of the data shown in (b). At high velocity, data collapse around a straight line, indicating that velocity decreases exponentially at short times. The solid line corresponds to a fit $V = V_0 e^{-t/\tau}$, with $\tau = 5.1 \pm 0.4$ ms.

$V = V_0 e^{-t/\tau}$ with $\tau = \frac{2\rho_s {R_0}^2}{9\eta_e}$. The slope measured in Fig. 5(c) yields a value $\eta_e = 230 \pm 15$ mPa s. This is much larger than both the viscosity of air and that of the foaming solution, as predicted by Schwartz and Princen.[22] This behavior is surprisingly simple, considering the large velocity of the impacting sphere and the complex rheological behavior of foams.

3.2.2 Final stage of deceleration. We now investigate the regime corresponding to the far right region of graph Fig. 5(c). Experimental points strongly deviate from a Newtonian behavior when V becomes smaller than 2 m s^{-1}, indicating that velocity in this region decreases faster than exponentially. To study this regime, we focus on our low velocity experiments ($V_0 < 5$ m s^{-1}), where we measure the position Z of the sphere, defined in Fig. 5(a) as the distance between the top of the sphere and the foam surface: at the moment of impact, $Z = 2R_0$.

In Fig. 6, we plot Z as a function of time and we observe that the sphere first sinks into the foam, reaches its maximal depth and then, instead of stopping at this point, "bounces" upwards. After a few oscillations, it stabilizes at a final position that is shallower than the maximal depth. Such rebounds of a projectile in a liquid have been observed in polymer and micellar solutions and interpreted as a signature of viscoelasticity.[23,24] Foams are also known to exhibit viscoelastic behavior. Elasticity in foams is due to the bubble's surface tension, since bubble deformations are equivalent to spring deformation, where the stiffness is given by surface tension.[25]

3.2.3 Foam deformation. To gain further insight at the way foam deforms around a projectile, we insert in a tank with flat transparent walls a foam in which several horizontal planes have been sprinkled with black particles. Seen from the side, the particle-seeded sheets appear as black lines. We image the deformation of these lines when a heavy sphere falls into the foam along the wall. As can be seen in Fig. 7, traces of the impact are only visible in a region close to the impact site, with a lateral extension of order R_0, suggesting that the size d of the gradient region is about R_0. Measurements of the velocity field around a moving plate in other yield stress fluids lead to the observation of a similar-sized boundary layer whose thickness does not depend on the plate velocity.[26]

In high velocity experiments, we also observe that some foam is entrained out of the tube by the sphere. For a 5 mm diameter polypropylene sphere and a velocity $V_0 \sim 20$ m s^{-1}, the amount of ejected foam is about 10 mg. Such a mass corresponds to that of a layer of thickness $\simeq R_0$ covering the bottom half of the

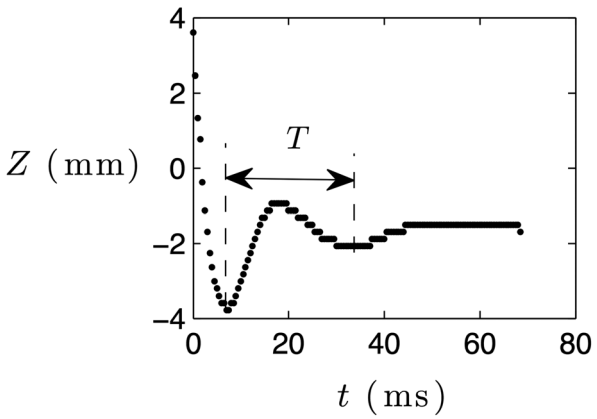

Fig. 6 Position of a polypropylene sphere ($R_0 = 2.4$ mm, $V_0 = 2.5$ m s^{-1}), as a function of time. Impact is followed by quickly damped oscillations of pseudo-period T.

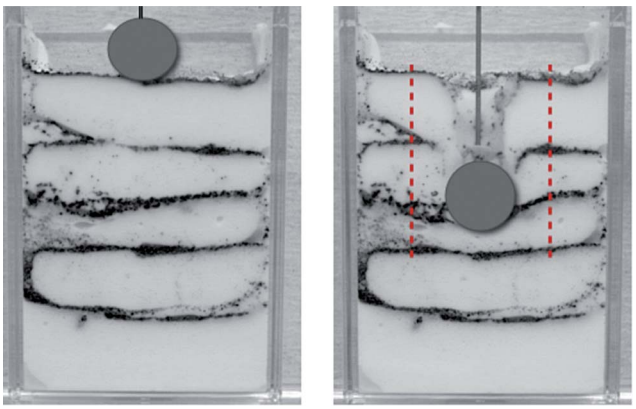

Fig. 7 To evaluate the extension of the region deformed by an impact, we prepare layer by layer a foam seeded with black particles, in a tank with flat transparent walls. We compare the shape of the black lines formed by these layers, viewed through the side wall, before and after the impact of a lead sphere of radius $R_0 = 3$ mm. We observe that the typical distance beyond which no deformation is visible, indicated by the red dashed lines, is comparable to the sphere radius.

sphere. This suggests that R_0 remains as a relevant scale for the flow around the sphere even at high velocity. It does not mean that deformation is limited to a tube of thickness R_0 around the projectile: as the sphere reaches the end of the tube, it crosses the foam surface, whose displacement is still visible more than three radii away from the axis of motion.

4 Interpretation and consequences

In this section, our purpose is to discuss the projectile dynamics. The equation of motion for a sphere decelerating in a foam is

$$M\frac{\mathrm{d}V}{\mathrm{d}t} = -\alpha\pi {R_0}^2\sigma \tag{1}$$

where σ represents the stress exerted by foam on the sphere and α a geometrical coefficient. The foam response is computed using a visco-elasto-plastic model from the literature,[27] presented in Appendix 6. Briefly, foam is characterized by three parameters: its elastic modulus μ, its macroscopic viscosity η_e, and an elasticity limit U_Y. The stress σ is the sum of an elastic term proportional to the deformation U and a viscous term proportional to the strain rate $\dot{\varepsilon}$:

$$\sigma = \mu U + \eta_e\dot{\varepsilon} \tag{2}$$

As sketched in Fig. 8, we describe the foam as a stack of visco-elasto-plastic layers of thickness R_0, each of them behaving according to the framework developed by Marmottant and Graner. The vertical motion of the sphere triggers the opening of a hole of radius R at the center of the viscoelastic layer, at a rate $\dot{R} = V$. We assume that the sphere only interacts with one layer at a time, and experiences a response given by eqn (2).

According to eqn (2), the stress σ depends on elastic deformation and strain rate. The strain rate $\dot{\varepsilon}$ is defined as the gradient of displacement in the foam and expressed as a ratio between the sphere's velocity and the typical size d of the gradient region: $\dot{\varepsilon} = \frac{\dot{R}}{d} = \frac{V}{d}$. Here we assume that the typical length d observed of order R_0 in Fig. 7 is the same in both radial and vertical directions, and that it does not vary with the sphere's velocity, as it is for Carbopol flowing around a plate.[26]

The sphere's position Z is given by $Z = R_0\int_0^t \dot{\varepsilon}(t')\mathrm{d}t'$. Together with eqn (10), this provides a closed system of equations that can be integrated numerically:

$$\begin{cases} \frac{1}{3}\rho_s {R_0}^2\ddot{\varepsilon} &= -\sigma \\ \sigma &= \mu U + \eta_e\dot{\varepsilon} \\ \frac{\mathrm{d}U}{\mathrm{d}t} &= 0 \text{ if } |U| > U_Y \text{ and } \dot{\varepsilon}U > 0 \\ \frac{\mathrm{d}U}{\mathrm{d}t} &= \dot{\varepsilon} \text{ else} \end{cases} \tag{3}$$

4.1 High velocity limit

Since $|U|$ is always smaller than U_Y, in the high velocity regime, the term in $\dot{\varepsilon}$ dominates in the rheological law: $\sigma \sim \eta_e\dot{\varepsilon} \sim \eta_e V/R_0$. The equation of motion can then be rewritten $M\frac{\mathrm{d}V}{\mathrm{d}t} = -\pi {R_0}^2\alpha\eta_e V/R_0$. The right-hand term can be identified as a Stokes force on a sphere decelerating in a viscous fluid, provided that we define an apparent viscosity η_{eff} such that $\alpha\eta_e = 6\eta_{\mathrm{eff}}$. As mentioned in Section 3, this equation leads to an exponential decay for the velocity $V = V_0\mathrm{e}^{-t/\tau}$ with $\tau = \frac{2\rho_s {R_0}^2}{9\eta_{\mathrm{eff}}}$, that successfully adjusts the data in Fig. 5(c). By measuring $\tau = 5.1$ ms on experimental curves, we find a foam viscosity $\eta_{\mathrm{eff}} = \frac{2\rho_s {R_0}^2}{9\tau} = 230$ mPa s. This value is much larger than the viscosities of the fluids comprising the foam, the gas ($\eta_g \sim 10^{-2}$ mPa s) and the foaming liquid ($\eta_l \sim 2$ mPa s). Similar values were obtained by Krishan *et al.* by fitting rheometry data acquired at frequencies between 1 and 80 Hz with a model assuming a viscous-like dissipation at high frequency.[28]

At the time of impact, the foam is still intact, so $U = 0 < U_Y$. According to eqn (3), U increases with the rate $\dot{\varepsilon}$. Because this strain rate is maximal at the beginning of the experiment, $\dot{\varepsilon}_0 = \frac{V_0}{R_0}$, U shortly reaches its maximal value U_Y. While $\dot{\varepsilon}$ progressively decreases, U sticks to the value U_Y, as predicted by Marmottant and Graner. During this phase, we have $\frac{\mathrm{d}U}{\mathrm{d}t} = 0$ and $\dot{\varepsilon} = \dot{\varepsilon}_P$. This implies that many plastic events are triggered during the deceleration and that, apart from the first few milliseconds following impact, no energy is stored in elastic deformation during this phase.

The fact that plasticity dominates the motion is confirmed by observations. After the sphere has crossed a tube filled with

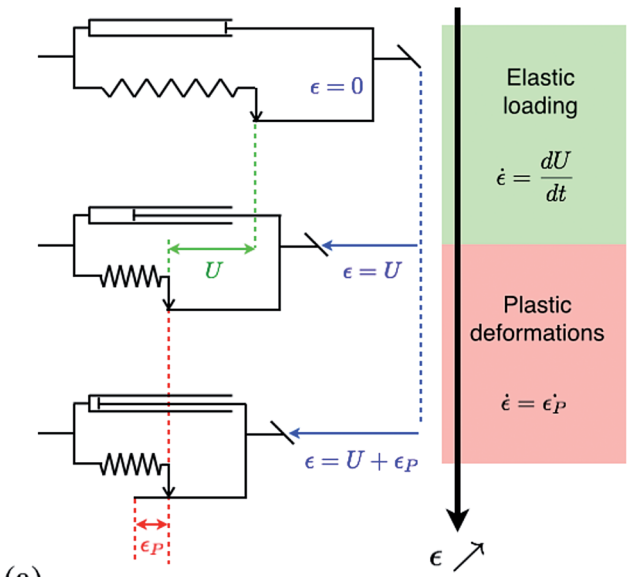

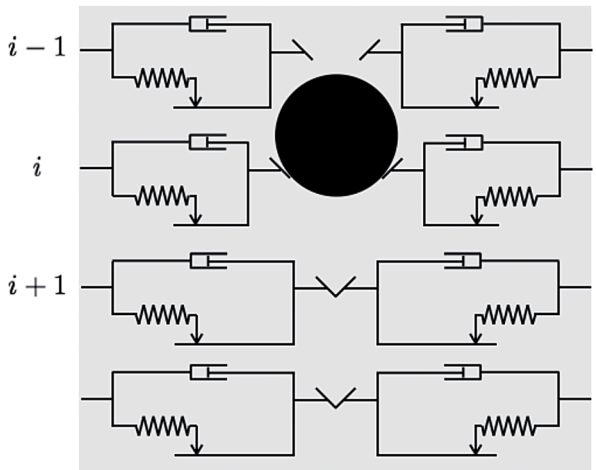

Fig. 8 (a) Behavior of a single elasto-visco-plastic cell under deformation ε. On the top image, the cell is at rest. There is no deformation, so $\varepsilon = 0$ and the spring has its equilibrium length, so $U = 0$. When ε starts increasing (middle picture), the spring compresses and absorbs all the deformation: $\varepsilon = U$. At this stage, deformation is purely elastic and $\varepsilon_P = 0$. When the spring reaches its limit of elasticity, U can no more increase and remain equal to U_Y. As represented in the bottom picture, any further deformation triggers plastic deformations. ε_P starts growing with the same rate as the total deformation $\dot{\varepsilon}_P = \dot{\varepsilon}$. (b) Sketch of a foam as an assembly of visco-elasto-plastic layers.

foam, it leaves a tunnel-shaped hole, similar to the one in the second picture of Fig. 7, whose diameter is slightly smaller than that of the sphere. The foam has been irreversibly damaged, and the material does not heal around the impact site.

4.2 Low velocity limit

At low impact velocities, or at the end of motion, the viscous contribution to the total stress can be neglected, so that eqn (2) reduces to: $\sigma \simeq \mu U$. Since $\dot{\varepsilon} = V/R_0$, the acceleration can be written $R_0\ddot{\varepsilon}$, which leads to

$$MR_0\ddot{\varepsilon} + 6\pi {R_0}^2 \mu U = 0 \quad (4)$$

Shortly after impact and during the initial deceleration phase, the elastic deformation U has a fixed value U_Y. As long as the sphere is moving downwards, $\dot{\varepsilon}$ and U have the same sign and $\frac{dU}{dt} = 0$. But when the sphere reaches its maximal depth, the sign of the velocity changes. This triggers elastic unloading and the deformation pattern switches again from plastic to elastic: $\dot{\varepsilon} = \frac{dU}{dt}$ and $\dot{\varepsilon}_P = 0$. Eqn (4) becomes that of a harmonic oscillator

$$MR_0 \frac{d^2U}{dt^2} + 6\pi {R_0}^2 \mu U = 0 \quad (5)$$

In the free regime, we expect oscillations of period $T_0 = 2\pi\sqrt{\frac{2\rho_s {R_0}^2}{9\mu}}$. We perform and image impacts with spheres of various size and density. We measure the period of oscillations as indicated in Fig. 6. The results are displayed in Fig. 9. As predicted, the period T increases linearly with the quantity $\sqrt{\rho_s {R_0}^2}$. From the slope a of this curve we can deduce an elastic modulus $\mu = \frac{8\pi^2}{9a^2} = 390$ Pa. This value is larger than those found in the literature for the shear modulus ($G \simeq 300$ Pa). Due to the scatter of experimental data, our measured value for μ is only a rough estimate. The precision $\Delta\mu/\mu$ on the elastic modulus is twice the relative error on the slope $\Delta a/a$. Using the slopes of the two blue lines in Fig. 9 as the extreme acceptable fits, we find $a = 150 \pm 10$ ms m$^{1/2}$ kg$^{-1/2}$ and therefore $\mu = 390 \pm 80$ Pa, still significantly larger than the shear modulus. This may be due to a complex combination of shear and compression. Then we would expect an elastic modulus comprised between the shear modulus G and the Young modulus E. Assuming the foam incompressible ($\nu = 0.5$), we can estimate $E = 2G(1+\nu) \simeq 900$ Pa. Our experimental value indeed belongs to this range.

4.3 Attenuation

We notice that oscillations are quickly damped. In order to comment on this, we rewrite the full equation of motion, including the viscous term:

$$\ddot{\varepsilon} + \frac{9\eta_{\text{eff}}}{2\rho_s {R_0}^2}\dot{\varepsilon} + \frac{9\mu}{2\rho_s {R_0}^2} U_Y = \frac{g}{R_0} \quad (6)$$

The coefficient of $\dot{\varepsilon}$ in eqn (6) can be identified as ω_0/Q, with $\omega_0 = 2\pi/T$ the pulsation of slow impact oscillations and Q the quality factor. We deduce a value for Q: $Q = R_0\sqrt{2\mu\rho_s}/3\eta_{\text{eff}} \simeq 2$, consistent with the high dissipation observed experimentally. In particular, a similar attenuation has been found for surface waves propagating radially away from the impact site.[29] The value we measured is actually that of a pseudo-period T and

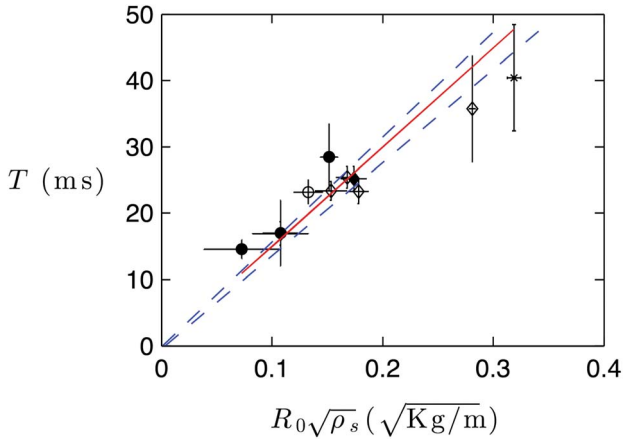

Fig. 9 Period of elastic oscillations T for spheres made of polypropylene (●), polyacetal (○), glass (◆), and heterogeneous materials (◇). The red line represents the best linear fit and yields a slope $a = 150$ ms m$^{1/2}$ kg$^{-1/2}$. The dashed blue lines stress the highest and lowest acceptable linear fits. 4 or 5 experiments are performed for each sphere type; vertical error bars represent mean period and standard deviation. The mass of the flag induces an error on density, taken into account by horizontal error bars.

differs from the period of free oscillations T_0 by a factor $\sqrt{1-\frac{1}{4Q^2}} \simeq 3\%$. Given the size of our error bars, we make a reasonable assumption when considering that $T \simeq T_0$ to estimate μ (Fig. 9).

4.4 Numerical results

Besides the asymptotic behaviors described above, we also performed a numerical integration of the system (eqn (3)), using Matlab and a least-square algorithm to numerically find a set of parameters minimizing the distance between an experimental and simulated curve $Z(t)$. We first tried to run the code with the values of η_{eff} and μ found experimentally in the previous paragraph, using U_Y as a free parameter. This led to solutions with exaggerated final oscillations. When letting free all three parameters, the most satisfying agreement was reached for $\eta_{\mathrm{eff}} = 220$ mPa s, $\mu = 164$ Pa and $U_Y = 0.415$ (Fig. 10).

The value for the viscosity coefficient is the same as the one obtained by fitting the high velocity experimental curves with a Newtonian model ($\eta_{\mathrm{eff}} = 230 \pm 15$ mPa s).

The elastic modulus, however, is two-fold smaller. An explanation for this may be that the elastic deformation does not take place in the immediate surrounding of the sphere: the sheared region around the projectile moves in a fluid way. This layer might generate a larger effective radius for the moving object.

In eqn (2), the viscous term dominates as long as $\dot{\varepsilon} > \mu U_Y/\eta_{\mathrm{eff}}$. This allows us to compute a velocity V^* below which an impact results in a response that is only a balance between elasticity and plasticity. We find that $V^* = \mu U_Y R_0/\eta_{\mathrm{eff}} = 0.7$ m s^{-1}. This is consistent with experimental observations, since the value of the velocity of the first outlier seen on the deceleration curve in Fig. 5(c) is 0.5 m s^{-1}.

4.5 Capture length

We now define the capture length $\mathscr{L}$ as the distance needed to stop a projectile, that is, the distance between the initial foam level and the lowest altitude of the bottom of the sphere. Experimental capture lengths are found by connecting high- and low-speed experiments with the velocity matching method presented in Section 2. Fig. 11 shows a comparison between the experimental capture length and the one predicted by the model for 5 mm polypropylene spheres. It takes about 15 cm of foam to stop a polypropylene sphere of radius 2.4 mm arriving at 40 m s^{-1}, that is, about 150 km h^{-1}.

Fig. 11 shows that $\mathscr{L}$ scales with the impact velocity V_0 on both experimental and numerical curves. Many data points are located to the right of the red curve. This can be seen as a signature of yield stress. Because the spheres used for this experiment are "floating", a finite velocity (about 2.5 m s^{-1}) is required for them to penetrate into the foam.

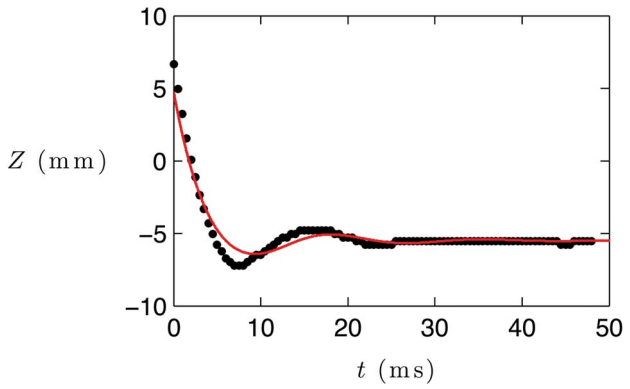

Fig. 10 Experimental (●) and numerical (red line) data showing the position $Z(t)$ of a polypropylene sphere ($R_0 = 5$ mm) penetrating at 3.3 m s^{-1} in a foam. Integration of eqn (3) is performed with the parameters: $\eta_{\mathrm{eff}} = 220$ mPa s, $\mu = 164$ Pa and $U_Y = 0.415$.

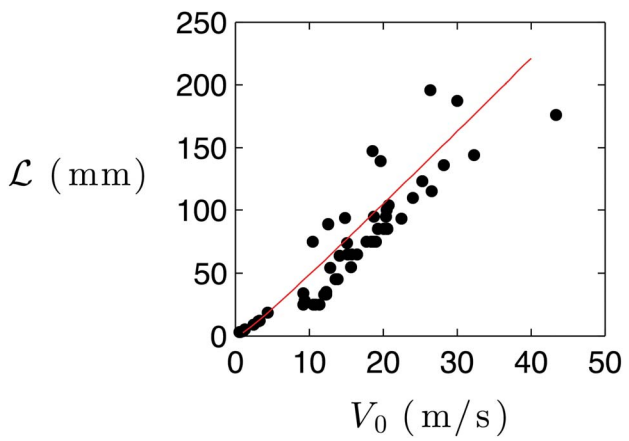

Fig. 11 Capture length $\mathscr{L}$ for a polypropylene sphere of radius $R_0 = 2.4$ mm, as a function of impact velocity V_0. Black dots represent experimental data and the solid line represents numerical predictions obtained with the following set of parameters: $\eta_{\mathrm{eff}} = 220$ mPa s, $\mu = 164$ Pa and $U_Y = 0.415$.

The same sphere hitting an air–water interface would decelerate in an inertial way: $M\mathrm{d}V/\mathrm{d}t \simeq 0.5\rho C_\mathrm{D}\pi {R_0}^2 V^2$. This leads to an exponential decrease of velocity $V = V_0 \mathrm{e}^{-z/z_i}$ with the inertial deceleration length $z_i = \frac{8}{3C_\mathrm{D}}\frac{\rho_\mathrm{s}}{\rho}R \simeq 9.4$ mm. In a more viscous fluid ($5 < \mathrm{Re}_0 = R_0V_0/\nu < 100$), we have shown that the typical deceleration scale is $z^* \simeq 1.3R_0\sqrt{\mathrm{Re}_0}\rho_\mathrm{s}/\rho \simeq 32$ mm.[21] A water layer of thickness z_i, or an oil layer of thickness z^*, is therefore sufficient to slow down the sphere. We can compare the mass of material needed to arrest spheres in a liquid foam and in other liquids. The ratio between specific masses of foam and water is the liquid volume fraction of foam Φ_l. We have:

$$\frac{M_\mathrm{foam}}{M_\mathrm{water}} = \frac{\Phi_\mathrm{l}\mathscr{L}}{z_i} \simeq 1.2 \quad (7)$$

$$\frac{M_\mathrm{foam}}{M_\mathrm{oil}} = \frac{\rho_\mathrm{water}\Phi_\mathrm{l}\mathscr{L}}{\rho_\mathrm{oil}z^*} \simeq 0.35 \quad (8)$$

This indicates that, regardless of the material used, the mass required to stop a projectile is roughly constant. In a Newtonian fluid, once the impact kinetic energy has been dissipated, the projectile is still subjected to buoyancy forces. Depending on its density, it will eventually stabilize either at the top or at the bottom of the fluid sample. In a yield stress fluid such as foam or Carbopol,[23] it reaches a finite equilibrium depth. In order to protect a surface from particle impacts with a Newtonian fluid, a tank of appropriate size is required, otherwise, whatever its initial thickness, the fluid sample will spread and become thinner. Yield stress fluids like foam can, to a certain extent, sustain their own weight. Samples as thick as several centimeters can stand as if they were solid.

For violent impacts, the energy dissipated in this phase can be so high that the particle gets damaged. This happens when interstellar particles collide at 5 km s^{-1} with a 3 cm thick aerogel.[30] To avoid destruction of fragile particles, materials with a density gradient can be used for inducing a progressive deceleration, for example foams with a gradient of liquid fraction. This strategy is employed in nature: the density of the foam-like material that constitutes the thick skin of pomelos gradually changes between the outer skin and the fruit flesh.[10]

4.6 Discussion

The most intriguing result of this study is the fact that a model assuming a constant viscosity for the foam seems to be relevant for a large part of our experiments, while classical foam rheology studies never report Newtonian behavior. Our experimental data can be fit with a Newtonian model as long as $\dot{\varepsilon} \gg \dot{\varepsilon}^* = V^*/R_0 \simeq 300\ \mathrm{s}^{-1}$. This means that the Newtonian regime can only be seen at values larger than 0.3 kHz, beyond the range classically explored in rheology experiments. Gopal and Durian[16] measured the apparent viscosity of Gillette foam in a Couette rheometer by imposing a constant shear rate. They found that apparent viscosity decreases with shear rate, with $\eta_\mathrm{eff} \simeq 500$ mPa s when $\dot{\varepsilon} = 300\ \mathrm{s}^{-1}$. Our experiments extend these data, and seem to suggest that viscosity at very high $\dot{\varepsilon}$ reaches a plateau (since we could understand our experiments at different $\dot{\varepsilon}$ with a single value for viscosity).

The model of Marmottant and Graner was initially written to describe quasi-static motion of foams. It is expected to break down when the strain rate $\dot{\varepsilon}$ becomes as large as the inverse of the microscopic relaxation time of the foam τ_relax. The exact composition of Gillette foam is not known, but measurements of surface rheology have shown that it behaves similar to surfactant solutions containing fatty acids as cosurfactants. Such mixtures exhibit a high surface modulus, meaning that surface tension takes a long time to go back to its equilibrium value after a change of interface shape or area. The relaxation time after a plastic event in Gillette foam is therefore quite long (about 0.2 s). This would lead to a limit $\dot{\varepsilon}_\mathrm{c} = 5\ \mathrm{s}^{-1}$ much lower than the typical values that we have at impact $\dot{\varepsilon}_0 \simeq 10\,000\ \mathrm{s}^{-1}$. However, the key feature of the model is the fact that the rate of plastic rearrangements is fixed by $\dot{\varepsilon}$. Marmottant and Graner assumed that this is true in the quasi-static case because $\dot{\varepsilon}^{-1}$ is the only available time scale in this regime. However, experiments on shear bubble clusters revealed that even beyond the quasi-static regime, the dynamics of a single plastic rearrangement is still governed by $\dot{\varepsilon}$.[31] This might explain why the model seems to function well even so far from its initial validity range.

5 Conclusions

Our first motivation was to quantify liquid foam's efficiency as a kinetic energy absorber. We show that a sphere can be stopped by a liquid foam, whatever its initial velocity, provided its mass-to-surface ratio is small enough to avoid sinking under its own weight. We proposed a simple model predicting the amount of foam needed to capture such a projectile, and showed that this quantity, for the spheres used in this study, corresponds to a foam sample size of about 20 cm. The idea of using liquid foams to slow down and confine solid particles seems to be promising. Particle capture takes advantage of the fluid nature of foams (during the viscous deceleration phase), as well as its ability to sustain its own weight and that of light projectiles. Understanding of the mechanical behavior of foams can help designing smart materials with heterogeneous properties that could adapt to the specific needs of a given application.

From a more fundamental point of view, we also report that a liquid foam, despite its complex heterogeneous structure, might behave like a Newtonian fluid at very high shear rates, in a range previously uncharted. Shooting in a foam gives access to its rheology, in a way that is not always possible in standard rheometers. We estimated the limits of this viscous-like behavior and show that it is restricted to frequencies of the order of, or above 0.2 kHz. A deep understanding of the value of this viscosity plateau would require further experiments, in which parameters such as the bubble size, volume fraction and surfactant chemistry would be varied. In the context of kinetic energy absorption, this would allow to adjust the foam's formulation to the specific needs of each application.

6 Appendix: visco-elasto-plastic model for foam flow

Foam is a complex fluid, exhibiting viscous, elastic and plastic behavior. Much work has been done and is still going on to properly describe its rheology.[7,32] When a foam is sheared, some bubbles are elastically stretched, but the structure can also be irreversibly modified by plastic events. Marmottant and Graner proposed to separate elastic and plastic contributions in the strain rate:[27]

$$\dot{\varepsilon} = \frac{\mathrm{d}U}{\mathrm{d}t} + \dot{\varepsilon}_{\mathrm{P}} \tag{9}$$

where U is the elastic deformation, that is, a state variable describing the current deformation state of the foam, while $\dot{\varepsilon}$ is the total strain rate and $\dot{\varepsilon}_{\mathrm{P}}$ is the plastic deformation rate. The rheological model is sketched in Fig. 8(a). The image at the top corresponds to a situation with zero deformation $\varepsilon = 0$. The spring is at rest, and its length is the equilibrium length. When the deformation ε increases, the spring compresses in a purely elastic way, resulting in a strain $\varepsilon = U$.

Plastic events occur when the amplitude of the elastic deformation reaches a yield value $\pm U_{\mathrm{Y}}$ and when it tends to increase, that is, when U and $\dot{\varepsilon}$ have the same sign. If the second condition is not fulfilled, the deformation may be large, but the strain rate leads to reversible elastic unloading. When plastic rearrangements occur, their rate is given by the only time scale in the problem, $\dot{\varepsilon}$, so $\dot{\varepsilon}_{\mathrm{P}} = \dot{\varepsilon}$. This results in the following equations for the elastic deformation

$$\begin{cases} \text{if } |U| > U_{\mathrm{Y}} \text{ and } \dot{\varepsilon} U > 0 \text{ then} & \dfrac{\mathrm{d}U}{\mathrm{d}t} = 0 \\ \text{otherwise} & \dfrac{\mathrm{d}U}{\mathrm{d}t} = \dot{\varepsilon} \end{cases} \tag{10}$$

The link between stress and strain is given by writing the stress σ as a sum of a viscous and an elastic component, with μ an elastic modulus, η_{e} a macroscopic viscosity and α a non-dimensional coefficient depending on the geometry of the system:

$$\sigma = \mu U + \alpha \eta_{\mathrm{e}} \dot{\varepsilon} \tag{11}$$

The material is therefore described by 3 parameters: its yield deformation U_{Y}, its viscosity η_{e} and its elastic modulus μ.

References

1 J. Plateau, *Statique Expérimentale et théorique des liquides soumis aux seules forces moléculaires*, Gauthier-Villars, 1873.
2 P. Sollich, F. Lequeux, P. Hébraud and M. Cates, *Phys. Rev. Lett.*, 1997, **78**, 2020–2023.
3 G. Katgert and M. van Hecke, *Europhys. Lett.*, 2010, **92**, 34002.
4 J. Banhart, *Prog. Mater. Sci.*, 2001, **46**, 559–632.
5 H. J. Schulze, *Physicochemical Elementary Processes in Flotation*, Elsevier Science Publishers, 1984.
6 C. J. Clark and E. M. Bennett, Method for explosive blast control using expanded foam, *US Pat.*, 4,589,341, 1986.
7 R. Höhler and S. Cohen-Addad, *J. Phys.: Condens. Matter*, 2005, **17**, R1041.
8 D. Weaire and S. Hutzler, *The physics of foams*, Oxford University Press, 1999.
9 L. Wang, J. T.-M. Cheung, F. Pu, D. Li, M. Zhang and Y. Fan, *PLoS One*, 2012, **6**, e26490.
10 M. Thielen, T. Speck and R. Seidel, *J. Mater. Sci.*, 2013, **48**, 3469–3478.
11 P. Tsou, *J. Non-Cryst. Solids*, 1995, **186**, 415–427.
12 A. Le Goff, L. Courbin, H. A. Stone and D. Quéré, *Europhys. Lett.*, 2008, **84**, 36001.
13 N. Louvet, R. Höhler and O. Pitois, *Phys. Rev. E: Stat., Nonlinear, Soft Matter Phys.*, 2010, **82**, 041405.
14 B. Dollet and F. Graner, *J. Fluid Mech.*, 2007, **585**, 181–211.
15 I. Cantat and O. Pitois, *Phys. Fluids*, 2006, **18**, 083302.
16 A. D. Gopal and D. J. Durian, *J. Colloid Interface Sci.*, 1999, **213**, 169–178.
17 N. D. Denkov, S. Tcholakova, K. Golemanov, K. P. Ananthpadmanabhanb and A. Lips, *Soft Matter*, 2009, **5**, 3389–3408.
18 H. Hoballah, R. Höhler and S. Cohen-Addad, *J. Phys. II*, 1997, **7**, 1215–1224.
19 F. Rouyer, S. Cohen-Addad and R. Höhler, *Colloids Surf., A*, 2005, **263**, 111–116.
20 H. Barnes and K. Walters, *Rheol. Acta*, 1985, **24**, 323–326.
21 A. Le Goff, D. Quéré and C. Clanet, *Phys. Fluids*, 2013, **25**, 043101.
22 L. W. Schwartz and H. M. Princen, *J. Colloid Interface Sci.*, 1987, **118**, 201–211.
23 H. Tabuteau, P. Coussot and J. R. de Bruyn, *J. Rheol.*, 2007, **51**, 125–137.
24 B. Akers and A. Belmonte, *J. Non-Newtonian Fluid Mech.*, 2006, **135**, 97–108.
25 H. M. Princen and A. D. Kiss, *J. Colloid Interface Sci.*, 1986, **112**, 427–437.
26 J. Boujlel, M. Maillard, A. Lindner, G. Ovarlez, X. Chateau and P. Coussot, *J. Rheol.*, 2012, **56**, 1083–1108.
27 P. Marmottant and F. Graner, *Eur. Phys. J. E: Soft Matter Biol. Phys.*, 2007, **23**, 337–347.
28 K. Krishan, A. Helal, R. Höhler and S. Cohen-Addad, *Phys. Rev. E: Stat., Nonlinear, Soft Matter Phys.*, 2010, **82**, 011405.
29 A. Le Goff, P. Cobelli and G. Lagubeau, *Phys. Rev. Lett.*, 2013, **110**, 236101.
30 M. J. Burchell, N. J. Foster, J. Ormond-Prout, D. Dupin and S. P. Armes, *Meteorit. Planet. Sci.*, 2009, **44**, 10.
31 A.-L. Biance, S. Cohen-Addad and R. Höhler, *Soft Matter*, 2009, **5**, 4672–4679.
32 D. Weaire, *Curr. Opin. Colloid Interface Sci.*, 2008, **13**, 171–176.

